Article

Developmental Cell

Pluripotency Surveillance by Myc-Driven Competitive Elimination of Differentiating Cells

Graphical Abstract

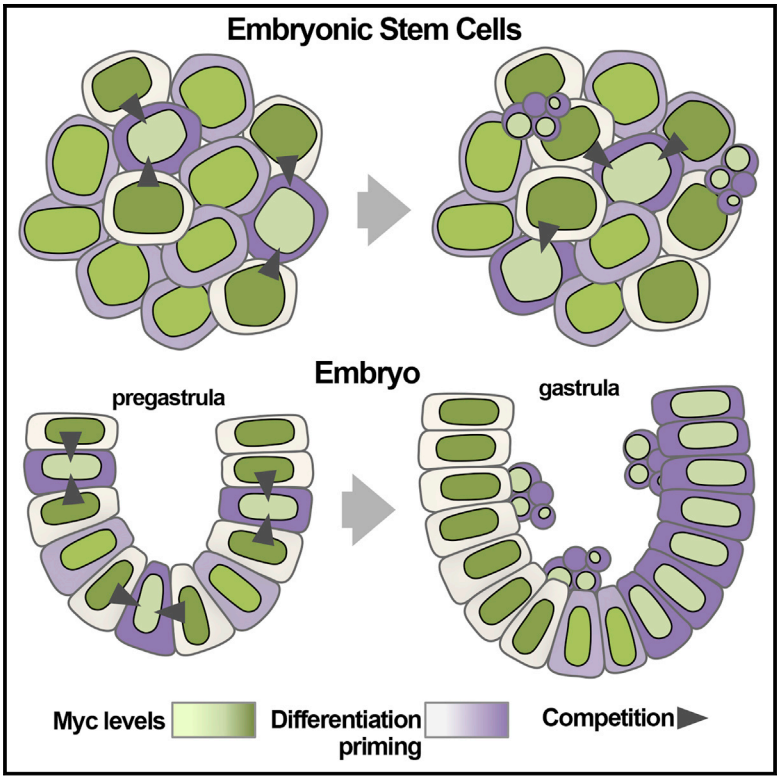

Authors

Covadonga Díaz-Díaz, Laura Fernandez de Manuel, Daniel Jimenez-Carretero, María Concepción Montoya, Cristina Clavería, Miguel Torres

Correspondence

mtorres@cnic.es

In Brief

Díaz-Díaz et al. show that Myc levels correlate with pluripotency and that this link triggers competitive interactions between naive cells (Myc-high) and cells starting differentiation (Myc-low). This mechanism allows embryos to maintain the purity of the pluripotent cell pool before the time is right for differentiation.

Highlights

- Transition from naive to primed pluripotent state drives Myc downregulation
- Myc-high naive cells eliminate Myc-low differentiating cells by cell competition
- Myc-low cells trigger apoptosis after persistent contact with Myc-high cells
- Myc-based competition eliminates differentiation-primed cells prior to gastrulation

Díaz-Díaz et al., 2017, Developmental Cell *42*, 585–599
September 25, 2017
http://dx.doi.org/10.1016/j.devcel.2017.08.011

Developmental Cell
Article

Pluripotency Surveillance by Myc-Driven Competitive Elimination of Differentiating Cells

Covadonga Díaz-Díaz,[1] Laura Fernandez de Manuel,[2] Daniel Jimenez-Carretero,[2] María Concepción Montoya,[2] Cristina Clavería,[1] and Miguel Torres[1,3,*]
[1]Cardiovascular Development Program, Centro Nacional de Investigaciones Cardiovasculares, CNIC, Madrid 28029, Spain
[2]Cellomics Unit, Centro Nacional de Investigaciones Cardiovasculares, CNIC, Madrid 28029, Spain
[3]Lead Contact
*Correspondence: mtorres@cnic.es
http://dx.doi.org/10.1016/j.devcel.2017.08.011

SUMMARY

The mammalian epiblast is formed by pluripotent cells able to differentiate into all tissues of the new individual. In their progression to differentiation, epiblast cells and their *in vitro* counterparts, embryonic stem cells (ESCs), transit from naive pluripotency through a differentiation-primed pluripotent state. During these events, epiblast cells and ESCs are prone to death, driven by competition between Myc-high cells (winners) and Myc-low cells (losers). Using live tracking of Myc levels, we show that Myc-high ESCs approach the naive pluripotency state, whereas Myc-low ESCs are closer to the differentiation-primed state. In ESC colonies, naive cells eliminate differentiating cells by cell competition, which is determined by a limitation in the time losers are able to survive persistent contact with winners. In the mouse embryo, cell competition promotes pluripotency maintenance by elimination of primed lineages before gastrulation. The mechanism described here is relevant to mammalian embryo development and induced pluripotency.

INTRODUCTION

The late preimplantation and early postimplantation mammalian embryo contains a population of pluripotent cells, the epiblast, able to differentiate into all tissues of the new individual (Rossant, 2008). Pluripotency is maintained in the mouse epiblast for several days before differentiation starts during gastrulation. In the progression from pluripotency to differentiation, initially naive epiblast cells transit through a differentiation-primed pluripotent state (Nichols and Smith, 2009). The naive pluripotent state is captured in embryonic stem cells (ESCs), which represent the *in vitro* counterparts of the early epiblast (Evans and Kaufman, 1981; Martin, 1981), while the primed pluripotent state is captured in epiblast stem cells (EpiSC) (Brons et al., 2007; Tesar et al., 2007) and epiblast-like stem cells (EpiLCs) (Hayashi et al., 2011), which represent the *in vitro* counterparts of the late epiblast. Whereas both pluripotent states share expression of a network of transcription factors known as the core-pluripotency network (Wang et al., 2006), they fundamentally differ in the signaling pathways they rely on. Naive pluripotency is promoted by leukemia inhibitory factor (LIF)/STAT3 (Smith et al., 1988) and BMP/SMAD (Ying et al., 2003) activation, while the primed state is maintained by FGF/MAPK and Activin/Nodal activation (Brons et al., 2007; Tesar et al., 2007).

Abundant cell death is observed during the different phases of epiblast development, with maximal incidence at 6 days of development, just before the onset of differentiation and gastrulation (Heyer et al., 2000; Plusa et al., 2008; Poelmann, 1980). This death peak is in part due to extreme sensitivity to DNA damage and mediated by a p53-dependent quality check (Heyer et al., 2000) and in part regulated by Myc levels (Clavería et al., 2013; Sancho et al., 2013). Both in the early mammalian embryo and in ESC cultures, a natural cell-to-cell heterogeneous pattern of Myc expression is found, and Myc-low cells are eliminated by apoptosis due to confrontation with Myc-high cells (Clavería et al., 2013; Sancho et al., 2013). This phenomenon, known as cell competition (CC), was first described in *Drosophila* epithelia, studying mutants that affect protein synthesis (Morata and Ripoll, 1975). In *Drosophila* and mammals, CC can be induced in different tissue contexts by discrepancies in Myc levels between otherwise viable neighboring cells (Clavería et al., 2013; de la Cova et al., 2004; Moreno and Basler, 2004; Villa del Campo et al., 2014).

In ESCs, Myc regulates cell metabolism and proliferation (Clavería et al., 2013; Gu et al., 2016; Hu et al., 2009; Kim et al., 2010; Scognamiglio et al., 2016) and promotes cell reprogramming to pluripotency in cooperation with transcription factors of the core-pluripotency network (Cartwright et al., 2005; Takahashi and Yamanaka, 2006), however, the biological role and dynamics of Myc-regulated endogenous CC in mammalian pluripotent cells remain unknown.

Here, we present for the first time live reporting of endogenous Myc levels and three-dimensional and temporal (3D + t) tracking of ESC colonies at cellular resolution to analyze the dynamics and biological basis of Myc-mediated competition in pluripotent mouse cells. We report that CC is driven by passive contacts between different ESC sub-lineages with contrasting Myc levels. While Myc regulation behaves autonomously in Myc-high cells, Myc-low cells respond to contact with winners with further progressive reduction of Myc levels. When these contacts are maintained for longer than a defined time period, Myc-low cells undergo apoptosis and become losers. Molecular and functional characterization of Myc-high and Myc-low

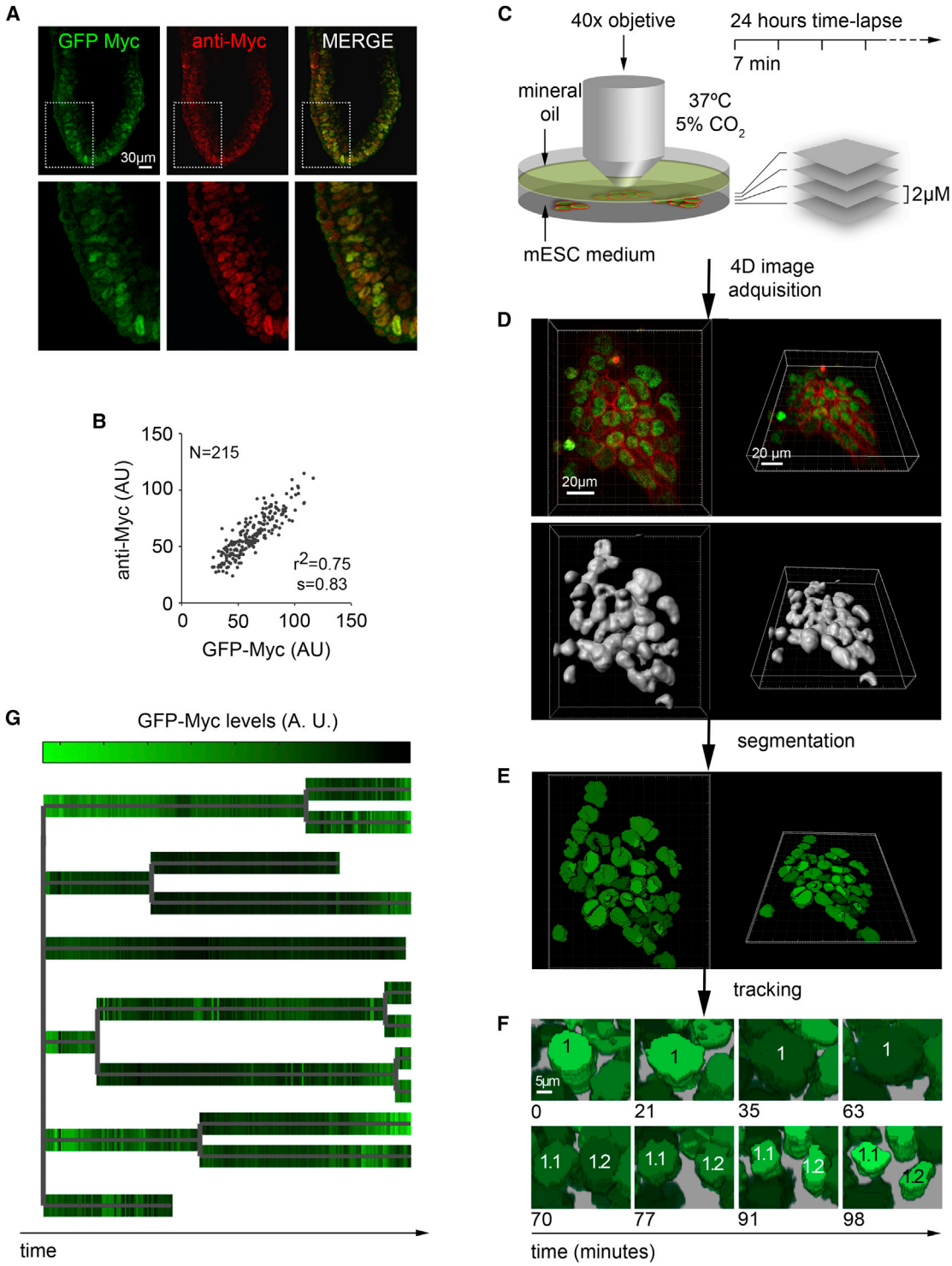

Figure 1. Multiparametric Four-Dimensional Analysis of Embryonic Stem Cells, Including Lineage Analysis and Tracking of Endogenous Myc Levels

(A) Confocal detection (optical sections) of Myc immunofluorescence and GFP native fluorescence in an E6.5 mouse embryo carrying the *GFP-Myc* knockin allele in heterozygosity. Frames of the whole epiblast are shown above, and magnifications of the areas indicated by the dotted rectangles are shown below.

(B) Quantification of the correlation between GFP and Myc immunofluorescence in single cells of the E6.5 epiblast.

(C) Live confocal microscopy setup.

(D) Example of 3D raw data acquisition from live GFP-Myc, membrane-Tomato ESCs (top), and whole volumes 3D rendering from these images (bottom).

(legend continued on next page)

ESC and epiblast cell populations shows that differentiation-primed Myc-low cells are eliminated by naive pluripotent Myc-high cells through CC. Our results reveal key aspects of endogenous CC dynamics in pluripotent cells and identify CC as a safeguard mechanism that maintains pluripotency in stem cell pools.

RESULTS

Tracking Endogenous Myc Levels in ESCs

To study the endogenous regulation of Myc and its role in spontaneous CC in ESCs, we derived a homozygous ESC line from previously described knockin mice expressing a GFP-Myc fusion protein (Huang et al., 2008). Myc protein (Cartwright et al., 2005) and mRNA (Dani et al., 1984; Hann and Eisenman, 1984) have very short half-lives, and therefore it was important to determine whether the GFP-Myc knockin line reported endogenous Myc levels. To this end, we studied the mouse embryo epiblast and found that GFP-Myc faithfully reported Myc levels in this tissue, despite the cell-to-cell highly heterogeneous Myc pattern (Clavería et al., 2013) (Figures 1A and 1B). In addition, we observed a very fast and strong variation in Myc levels during mitosis in ESCs (Figure S1). Both Myc and GFP-Myc levels decreased drastically in the transition from prophase to metaphase, remained undetectable during metaphase, anaphase, and cytokinesis, and increased sharply during telophase (Figure S1). The sharp decrease in Myc/GFP-Myc levels at mitosis initiation matches an increase in T58 phosphorylation, which targets Myc for degradation (Welcker et al., 2004). T58-phosphorylated Myc, however, was not detected during interphase (not shown), indicating mitosis-specific degradation of Myc. These observations show that the GFP-Myc knockin line faithfully reports endogenous Myc levels, even through phases of rapid Myc degradation and re-synthesis.

We next performed 24 hr 3D + t tracking experiments to characterize Myc dynamics during spontaneous CC. Cells move very actively in ESC colonies (Movie S1), so that 3D scans were required every 7 min for accurate cell tracking (Figure 1C). To facilitate detection of cell contours, we stably transfected GFP-Myc cells with constitutively expressed tdTomato. Red and green channels were acquired, respectively reporting the cell membrane and the GFP-Myc fusion (Figure 1D). We developed a computer workflow for automatic 3D + t segmentation and tracking, assisted by manual inspection and correction (Figure 1E and STAR Methods). This approach allowed cell-lineage tracing across cell division, so that information on progenitor-cell identity was incorporated to daughter-cell identities, generating lineage trees (Figure 1F; Movies S2 and S3). We thus obtained lineage trees for every cell family in the studied colonies, together with multiple quantitative parameters, including cell and nuclei trajectories, volumes, shapes, GFP levels, and neighborhood information (Figure 1G, see also raw data availability in STAR Methods).

Myc Expression Levels Define Sub-lineages in the ESC Population

To understand the nature of Myc-level heterogeneity in ESCs, we aimed first to determine the stability of Myc levels during tracking. Classification of the whole cell population into three groups according to mean GFP-Myc level (top 30%, Myc-high (H); lower 30%, Myc-low (L); the rest, Myc-medium (M)) showed that Myc-H cells have 2.5× higher GFP-Myc intensity than Myc-L cells (Figure 2A). Given that Myc-level heterogeneity is the driver of spontaneous CC (Clavería et al., 2013), we studied the dynamics of this heterogeneity. First, we determined cell-cycle-dependent Myc fluctuations, for which we performed *in silico* synchronization of the cell cycle. The resulting expression profile captures the drastic reduction of GFP-Myc levels during mitosis and the rapid recovery during telophase (Figures 2B and S1). In addition, a moderate increase in Myc levels precedes mitosis, and typical fluctuations are detected afterward (Figure 2B). Although drastic, the fluctuations during mitosis span a very short portion of the cell cycle and therefore do not account for the observed cell-to-cell heterogeneity in GFP-Myc levels (Figure 2A). Examination of the stability of Myc-level groups revealed little variation during the 24 hr tracked (Figure 2C), even through cell division (Figure 2D) and despite Myc degradation and re-synthesis during mitosis. These results suggest that Myc levels are imprinted to some extent in ESC sub-lineages, such that they are largely conserved through mitosis. To test this observation during a longer tracking period, we performed retrospective clonal analysis in ESCs and determined the variability of Myc levels within clonally related cells and in randomly chosen equivalent groups. For this study, we used the *RERT* knockin, which provides ubiquitous and tamoxifen-inducible Cre activity (Guerra et al., 2003), in combination with the *iMOS*^{WT} Cre reporter, which provides mosaic activation of EYFP/ECFP (Clavería et al., 2013). For clonal analysis, the tamoxifen dose was titrated to achieve low-frequency recombination. This study showed that Myc levels display much lower variation in clonally related cells than in randomly chosen cells, with an estimated heritability of 0.8 per cell division (Figures 2E and 2F). In addition, we sorted Myc-H and Myc-L cell populations to study the stability of Myc levels in these populations. Myc-H cells slowly regenerated the original expression levels, reaching a distribution close to the original 3 days after sorting (Figure 2G). In contrast, Myc-L cells died as a consequence of the replating procedure, precluding Myc levels tracking (not shown).

The cell-to-cell heterogeneous pattern, the high heritability of Myc levels, and the slow regeneration of Myc levels from Myc-H cells indicate that different sub-families of Myc expression levels coexist in ESC cultures and largely transmit their Myc levels to their progeny. Myc heterogeneity is thus different from that reported for Nanog, which is characterized by stochastic transitions between Nanog-high and Nanog-low states (Chambers et al., 2007; Kalmar et al., 2009). In fact, we observed no significant correlation between Myc and Nanog levels in ESCs (not shown).

(E) 3D segmentation of the nuclei of the ESC colony in (D), with GFP-Myc levels displayed as green brightness intensity.
(F) Example of the tracking of segmented nuclei during mitosis.
(G) Cell-lineage tree deduced from the tracking data, displaying the temporal pattern of GFP-Myc levels.
See also Figure S1.

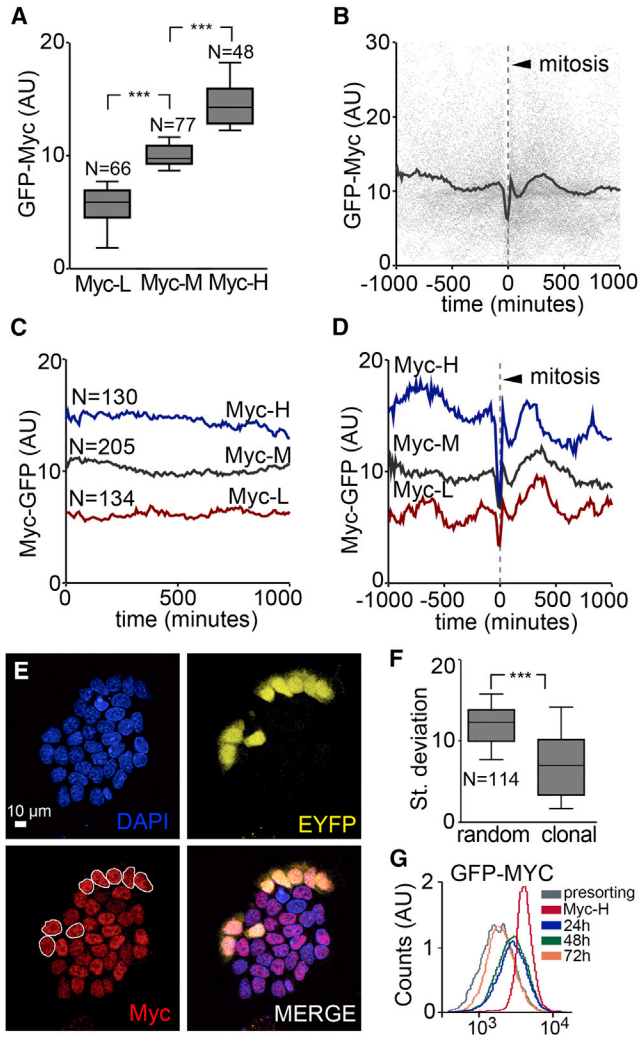

Figure 2. Heritability of Myc Levels in ESC Cultures

(A) Distribution of GFP-Myc levels after *in silico* classification of ESCs into groups according to live-recorded average GFP-Myc levels before cell's first division.

(B) Display of individual (dots) and spline smooth line (SSL) of GFP-Myc levels of all dividing cells synchronized to cell division.

(C) Tracking of GFP-Myc levels (SSLs) in Myc-H, Myc-M, and Myc-L ESCs.

(D) Similar data to (C), synchronized to cell division time.

(E) Example of a clonal mark induced by $iMOS^{WT}$ activation in an ESC colony together with immunofluorescence detection of Myc levels.

(F) Variation of Myc levels in clonal groups and equivalent groups of randomly chosen cells.

(G) Cytometry analysis of Myc levels in the original population and the Myc-H sorted population at different times from plating.

Boxplots show median, 25th and 75th percentiles (boxes), 10th and 90th percentiles (whiskers). Mann-Whitney test was used for statistical analysis. ***$p < 0.0001$.

Spontaneous ESC Competition Is Driven by the Sensitivity of Losers to Time in Contact with Winners

We next used nearest-neighbor analysis to study how Myc heterogeneity leads to CC in ESCs. First, we used two different live tracers of apoptosis (Hoechst58 and a caspase-3 activity reporter) to identify apoptosis events in time-lapse analysis (Movies S4 and S5). This analysis allowed us to identify a characteristic membrane collapse that takes place during apoptosis and allows identification of apoptotic events without using specific reporters (Movies S6 and S8). Using membrane collapse detection, we identified 24 apoptotic cells (prospective dying cells [PDCs]) during time-lapse analysis of GFP-Myc cells. The mean GFP-Myc level in PDCs during tracking was lower than that in the non-dying cells (NDCs) (Figure 3A), and approximately matched the levels observed in Myc-L cells (Figure 2A), which agrees with previous analyses of Myc-mediated competition (Clavería et al., 2013; Sancho et al., 2013). When inspecting the individual profiles of GFP-Myc expression in PDCs, we found that 3 of the 24 apoptotic events affected cells with high or medium Myc levels and therefore were considered unrelated to Myc-driven CC and excluded from further analysis. These observations indicate that the majority of spontaneous apoptotic events in ESC cultures correlate with low Myc expression levels.

Next, we synchronized *in silico* the temporal profile of PDC GFP-Myc levels to the time of PDC death and compared this profile with that of NDCs (Figure 3B). We observed continuously lower Myc levels in PDCs than in NDCs, indicating that preexisting low Myc levels correlate with the loser fate. Interestingly, this synchronization also revealed a sustained reduction of GFP-Myc level in PDCs beginning 500 min before death (Figure 3B). For comparison, we characterized the group of cells that show Myc levels similar to those found in PDCs but do not die during the observation time (Myc-L non-dying cells [ML-NDCs]). ML-NDCs also showed persistently lower Myc levels than the general population during the observation time but did not show any tendency toward a reduction in GFP-Myc levels (Figures S2A and S2B).

We next analyzed the behavior of Myc levels in PDC neighbors. GFP-Myc levels of PDC neighbors were initially lower than those of NDCs, but from 800 min before loser death they rose until matching the levels of NDCs, subsequently maintaining a plateau until PDC death (Figures 3C–3E). The increase in GFP-Myc levels of PDC neighbors therefore precedes the decline in PDC GFP-Myc levels. In contrast, neighbors of ML-NDCs stably maintain lower levels than NDCs (Figure 3F). Furthermore, ML-NDCs do not experience increases in GFP-Myc levels of neighbors extending longer than 500 min (Figure 3G). The difference in GFP-Myc levels between a PDC and its neighbors is thus exacerbated before the death event, so that their contrast in GFP-Myc levels with neighbors is always below that preceding PDC death (Figure S2C). These results indicate that Myc-low cells survive in ESC colonies as long as the discrepancy in Myc levels with neighbors is moderate; however, sustained high discrepancy for periods above 600–800 min result in their elimination. The fact that the profile of PDC neighbors forms a plateau indicates that the feature associated with loser cell death is time of exposure to neighbors with Myc levels above a discrepancy threshold and not accumulated Myc discrepancy. If accumulated Myc discrepancies were measured by loser cells, then shorter exposures to higher Myc levels in neighbors would also lead to loser cell death, and a sustained increase in average Myc levels of PDC neighbors would have been observed instead of a plateau.

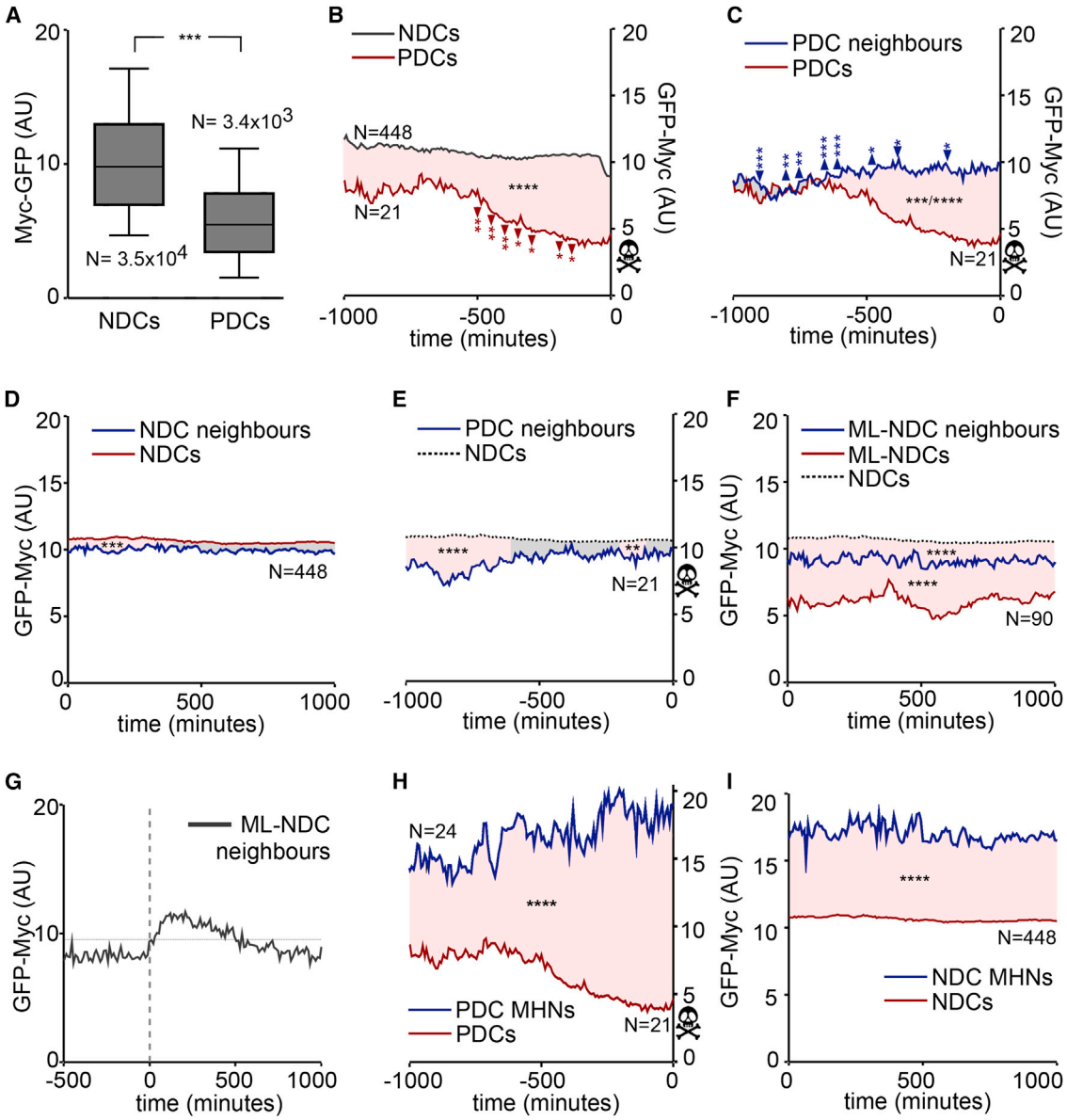

Figure 3. Live Analysis of Cell Competition in ESC Cultures

(A) Distribution of GFP-Myc levels during 24 hr live analysis of prospective dying cells (PDCs) and non-dying cells (NDCs).

(B) Temporal evolution of GFP-Myc levels in PDCs and NDCs, synchronized to the time of cell disappearance (death for PDCs and division for NDCs). Significant decreases between consecutive 100 min sections are shown (arrowheads).

(C) Temporal evolution of GFP-Myc levels in PDCs and PDC-neighbor means synchronized to PDC death. Significant increases between consecutive 100 min sections are shown (arrowheads).

(D) Temporal evolution of GFP-Myc levels in NDCs and their neighbor (means).

(E) Temporal evolution of GFP-Myc levels in NDCs and PDC-neighbor means.

(F) Temporal evolution of GFP-Myc levels in Myc-L non-dying cells (ML-NDC), ML-NDC neighbor means, and NDCs.

(G) GFP-Myc levels of ML-NDC neighbors synchronized to the initiation of periods in which their mean level is equal to or higher than that shown by PDC neighbors before PDC death. Vertical dotted line indicates synchronization time. Horizontal line indicates the average levels of PDC neighbors during the plateau preceding PDC death.

(H) Temporal evolution of GFP-Myc levels in PDCs and their Myc-highest neighbor (PDC-MHN).

(I) Temporal evolution of GFP-Myc levels in NDCs and their Myc-highest neighbor (NDC-MHN).

(B–I) Display SSLs. Pink areas between graph lines in (B)–(F), (H), and (I) indicate p values < 0.01. Boxplot in (A) shows median, 25 and 75 percentiles (boxes), 10 and 90 percentiles (whiskers). Mann-Whitney test was used for statistics, ***$p < 0.0001$. Statistical analyses in (B)–(F), (H), and (I) were performed by comparing 100-min sections between the represented datasets, using a Wilcoxon matched-pairs signed rank test for comparing PDCs, NDCs, and ML-NDCs with their neighbors and a Mann-Whitney test for the rest of the comparisons. Longitudinal changes of PDCs and PDC neighbors shown in (B) and (C) were studied using a Mann-Whitney test to determine significant changes between consecutive 100-min sections centered at 50-min sliding positions. Transitions between consecutive temporal sections showing significant differences are shown by an arrowhead and indicate the p value. *$p < 0.05$, **$p < 0.01$, ***$p < 0.001$, ****$p < 0.0001$. See also Figure S2.

Passive Contacts between ESC Sub-lineages with Preexisting Discrepancy in Myc Levels Drives Cell Competition

The first event anticipating loser cell fate is thus the increase in a neighbor's Myc level; we therefore studied the nature of this increase. The results observed could correspond to replacement of neighbors by cells with Myc levels higher than their own, or to Myc upregulation in persisting neighbors. To distinguish these possibilities, we inspected individual GFP-Myc profiles of PDC neighbors and found that the increase in aggregate GFP-Myc levels of neighbors corresponds to the establishment of new contacts with outstanding neighbors with high GFP-Myc levels (Myc-highest neighbors [MHN]; see examples in Figure S2D). The temporal profile of GFP-Myc level in MHNs was similar to that for all neighbors but with a wider discrepancy in GFP-Myc levels (Figures 3H and 3I). The total number of MHN contacts contributing to the GFP-Myc plateau and the duration of these contacts are highly variable (Figures 4B and S2D), indicating that MHNs do not engage in the interaction with PDCs. In addition, the complete GFP-Myc temporal profiles show that Myc levels in PDC neighbors are insensitive to contact with PDCs (Figures 4A and S2E) and unrelated to cell-cycle phase (Figure 4B). Furthermore, the distribution of the duration of PDC contacts with their MHNs is similar to that observed with their Myc-low neighbors (Figure 4C), indicating no specific pattern of direct contacts between prospective winner and loser cells. We also observed no correlation between GFP-Myc levels and the motility of ESCs during spontaneous CC (Figure S3).

These results indicate that Myc levels in winner cells behave autonomously during CC and that neighbor exchange, not Myc regulation, produces the increase in GFP-Myc levels that precedes death events (see example in Movie S7).

Our results show that loser cell death takes place when accumulated individual contacts lead to high discrepancy in neighbor Myc levels sustained for longer than 600–800 min. In addition, a progressive decrease of Myc levels was observed preceding loser cell death. To test these observations, we experimentally induced CC using the *iMOS*$^{T1\text{-}Myc}$ allele (Clavería et al., 2013) to induce mosaic overexpression of EYFP-Myc in ESC colonies. We then studied the temporal profile of EYFP induction and apoptosis in time lapse. In accordance with the analysis of spontaneous CC, the cell-death rate in wild-type (WT) cells neighboring EYFP-Myc-expressing cells increased by more than 5-fold 600 min after the onset of EYFP-Myc induction (Figures 4D–4G and Movie S8). In contrast, the apoptosis rate in WT cells not neighboring EYFP-Myc cells remained stable during EYFP-Myc cell induction (Figure 4G). To study the evolution of Myc levels in neighbors of EYFP-Myc-activated cells, we repeated similar experiments in co-cultures of *iMOS*$^{T1\text{-}Myc}$ and GFP-Myc ESCs and traced Myc levels in EYFP-Myc neighbors. We observed that neighbors of EYFP-Myc cells that died during tracking showed a sustained decrease in Myc levels starting shortly after EYFP-Myc induction (Figures 4H–4K). In contrast, neighbors of EYFP-Myc cells that did not die during tracking showed higher initial Myc levels than dying cells and maintained these levels during observation (Figures 4H–4K). These results confirm the conclusions from the live analysis of spontaneous CC. Furthermore, they show that direct contact between winner and loser cells is required during Myc-induced CC, which suggest that fitness comparison takes place through direct contact between winners and losers in ESC cultures.

Proliferation Correlates with Myc Levels but Not with ESC Competitive Ability

We next studied the biological significance of the different Myc levels in ESCs sub-lineages. Previous work showed the cooperative role of *Mycn* and *Myc* in maintaining the ESC proliferative program (Scognamiglio et al., 2016). We observed that Myc-L cells indeed proliferate less, showing a much lower fraction of the population in S phase than Myc-H cells and accumulation in G1 (Figure 5A). In addition, Myc-L cells showed a larger fraction of cells that did not divide during tracking in comparison with Myc-M or Myc-H cells (Figure 5B). In contrast, no difference was found in the proliferative activity of Myc-H and Myc-M populations (Figure 5B), and GFP-Myc levels are similar between cells that divided once and those that divided twice during the observation period (Figure 5C). In addition, we tracked cell-cycle progression by measuring nuclear volume (Figure 5D). This analysis showed that nuclear size in proliferating cells increased linearly during interphase and halved during mitosis (Figure 5D). This observation indicates that the increase in nuclear size reports S phase. The temporal profile of nuclear size revealed similar cycling speeds for proliferating cells, irrespective of their belonging to the Myc-H, Myc-M, or Myc-L groups (Figure 5E). These results show that ESCs require a minimum amount of Myc to enter the proliferative status, but once the proliferative status is achieved, Myc levels do not determine cell-cycle speed. In addition, these results show that the Myc-L population is composed of cells that proliferate at equal rates with Myc-H and Myc-M populations and cells that do not proliferate. Importantly, both dividing and non-dividing Myc-L cells showed substantially increased apoptosis rates, indicating a direct correlation between Myc levels and competitive ability, irrespective of the proliferative status (Figure 5F).

Transcriptomic Analysis of ESCs According to Endogenous Myc Expression Levels

Examination of the transcriptome of ESCs with different GFP-Myc levels revealed the most significant difference to be pluripotency network regulation. Gene set expression analysis indicated that eight of the top ten hits in gene sets from experiments in ESCs identified targets of pluripotency factors (p values between $<3.78^{-25}$ and $<1.73^{-62}$) (Figure 6A). Additional gene sets not shown in Figure 6 included SALL4-bound genes, RAR-bound genes, and Elongin-A targets. While SALL4 is a known pluripotency factor, RAR-bound genes include genes involved in both differentiation and pluripotency (Delacroix et al., 2010), and Elongin-A is an RNA elongation factor regulating gene expression related to cell-cycle progression in ESCs (Yamazaki et al., 2003).

Additional analyses specific for genes preferentially expressed in Myc-L cells identified several pathways of potential interest (Figure S5). The gene sets identified included metabolic pathways, such as glycolysis- and hypoxia-related genes. In addition, pathways potentially related to differentiation were also identified, such as estrogen receptor, TNF-NFkB, IL2-STAT5, Epithelial-Mesenchymal transition, and apical junction components. Most interesting to our characterization, the p53 pathway

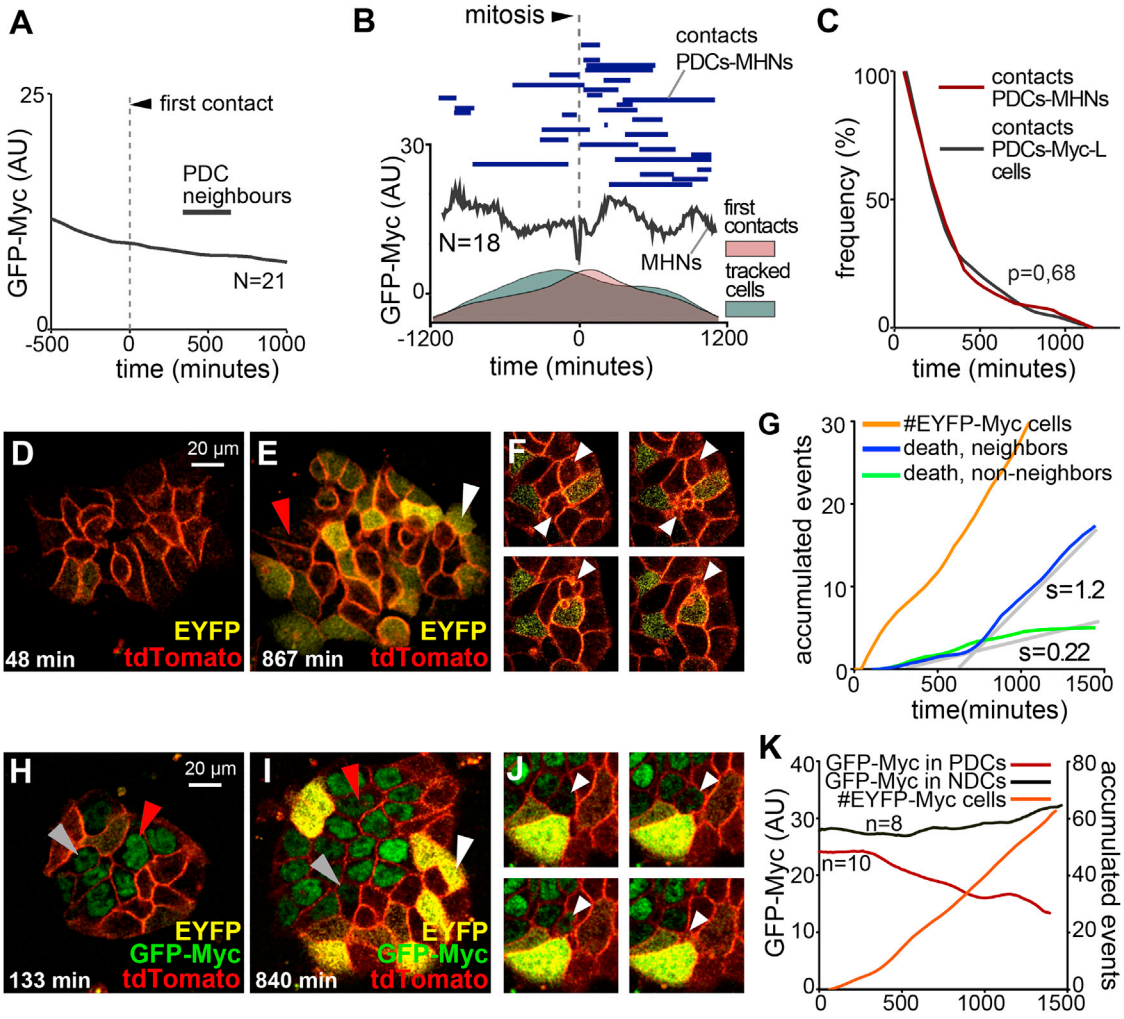

Figure 4. Dynamics of Winner-Loser Cell Interactions and Myc-Level Regulation during ESC Competition

(A) Temporal evolution of mean GFP-Myc levels in PDC neighbors synchronized to the time of their first contact with a PDC.

(B) GFP-Myc levels of PDC-MHN synchronized to cell division (line), together with contact periods of PDC-MHN with PDCs (bars, top), and temporal profiles of first contacts and number of tracked cells.

(C) Frequency profile of the duration of the periods of contact between PDCs and their MH-N and their Myc-L neighbors.

(D and E) Confocal images showing the EYFP pattern in *iMOS*$^{T1\text{-}Myc}$ ESCs at two time points, 48 min (D) and 867 min (E), during time-lapse analysis after conditional activation. EYFP reveals cells overexpressing Myc. Red arrowhead in (E) indicates negative cells and white arrowheads in (E) indicate EYFP-Myc cells.

(F) Selected frames from live analysis of *iMOS*-induced CC showing apoptosis of non-activated cells neighboring activated *iMOS*$^{T1\text{-}Myc}$ cells. Arrowheads indicate cells that die during observation.

(G) Cumulative temporal representation of EYFP activation events and cell death events in non-EYFP cells neighboring or not neighboring EYFP-Myc cells following *iMOS*$^{T1\text{-}Myc}$ activation. s, slope (events/hour).

(H and I) Confocal images showing the EYFP and GFP-Myc patterns in mixed ESC colonies from 1:1 co-culture of *iMOS*$^{T1\text{-}Myc}$ and GFP-Myc ESCs. Images represent two selected time points, 133 min (H) and 840 min (I), from the time-lapse analysis after conditional activation of *iMOS*$^{T1\text{-}Myc}$ with tamoxifen. Widespread EYFP reveals cells overexpressing Myc, and nuclear GFP reveals GFP-Myc cells. White arrowhead indicates EYFP-Myc cells, gray arrowheads indicate a PDC and red arrowheads indicate an NDC, both neighbors of EYFP-Myc cells.

(J) Selected frames from live analysis of *iMOS*-induced CC showing apoptosis of GFP-Myc cells neighboring activated *iMOS*$^{T1\text{-}Myc}$ cells. Arrowheads indicate cells that die during observation.

(K) Cumulative temporal representation of EYFP activation events and GFP-Myc levels in PDC and NDC neighbors of EYFP-Myc cells in *iMOS*$^{T1\text{-}Myc}$/GFP-Myc mixed ESC cultures following *iMOS* induction.

(A), (C), (G), and (K) display locally weighted scatterplot smooth lines and (B), SSL. See also Figures S2 and S3.

and the apoptosis pathway were identified (Figure S5). The identification of genes that regulate apoptosis and p53 correlates well with the presence of losers within the MYC-L class. p53 protein detection in GFP-Myc ESCs confirmed higher expression levels in apoptotic cells of the Myc-L population (Figures S6A and S6B), however we did not observe correlation between

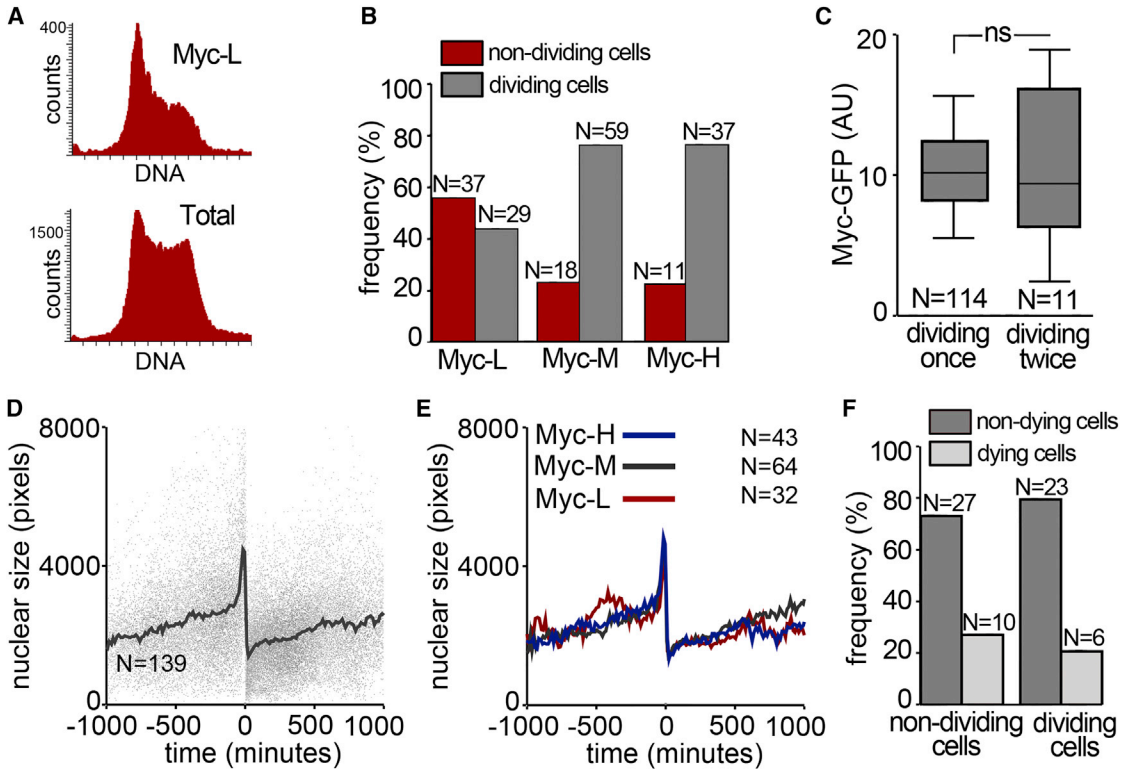

Figure 5. Myc Levels and Proliferation in ESCs

(A) DNA content cytometry profiles.

(B) Percentage of dividing and non-dividing cells during time-lapse analysis in ESCs classified according to Myc levels.

(C) Average GFP-Myc levels in ESCs dividing once or twice during tracking.

(D) Display of individual (dots) and SSL of nuclear size tracking in dividing cells synchronized to cell division time (t0).

(E) Similar data as in (D), in ESCs classified by Myc levels.

(F) Frequency of apoptosis in Myc-L ESCs according to their proliferative behavior during tracking.

Boxplots show median, 25th and 75th percentiles (boxes), 10th and 90th percentiles (whiskers). Mann-Whitney test was used for statistical analysis. ns, $p > 0.05$. See also Figure S1.

DNA damage and Myc levels (Figures S6C and S6D), indicating that p53 activation during CC does not result from a DNA damage response. These observations suggest that p53 activation in Myc-L cells is involved in CC-induced apoptosis in ESCs. In this study, we concentrated our analysis on the relationship between pluripotency, Myc levels, and CC.

The Pluripotency Status Determines Myc Expression Levels and ESC Competitive Ability

We further examined the connection of Myc levels to pluripotency by comparing the transcriptomes Myc-H, Myc-M, and Myc-L cells with those of the naive and primed pluripotent states previously described in ESCs and EpiLCs (Buecker et al., 2014; Sasaki et al., 2015). Principal component analysis and examination of the main regulators of pluripotency status (Martello and Smith, 2014) showed that Myc-H cells were closest to naive ESCs, whereas Myc-L cells approximated the differentiation-primed EpiLC-like expression profile and Myc-M cells showed an intermediate position (Figures 6B–6D). These results indicate that Myc levels correlate with the transcriptome changes that take place in the transit between the naive and primed pluripotency states. These observations are consistent with our experimental ESC culture conditions (serum replacement + LIF without feeders, see STAR Methods), which allow heterogeneity in pluripotency status. The results are also consistent with the substantial heritability of Myc levels, since transition from the naive to the primed pluripotent state is limited by LIF, and the primed pluripotency status is not reversible by changes in the signaling environment (Guo et al., 2009).

We then checked Myc levels in correlation with activation of the two main signaling pathways that characterize the naive and primed pluripotency status. We found that ESC GFP-Myc levels negatively correlate with activation of pERK (Figures 6E and 6F), whose activity supports acquisition and maintenance of the primed state (Kunath et al., 2007), but positively correlate with activation of pSTAT3 (Figures 6G and 6H), which characterizes and promotes the naive state (Niwa et al., 1998; van Oosten et al., 2012). These observations further support that the differentiation status correlates with endogenous Myc levels in ESC cultures and suggest that differentiation-primed lineages might be outcompeted by their naive neighbors. To directly test this hypothesis, we confronted differentiating ESCs with naive ESCs. Differentiating ESCs were induced by changing cells from medium supplemented with LIF to medium without LIF. Naive

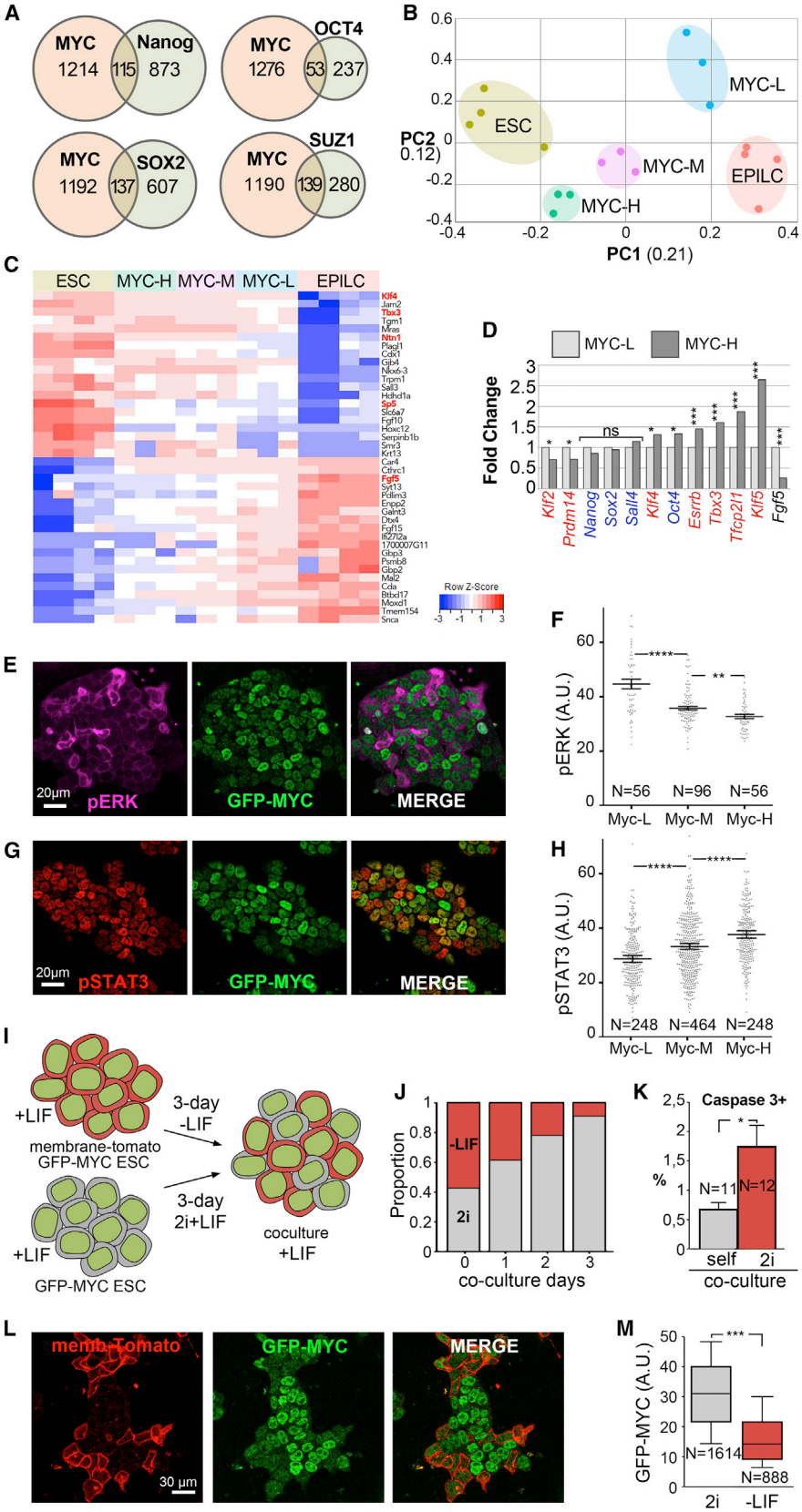

(legend on next page)

cells were obtained by adding "2i" (MAPK and GSK3 inhibitors) (Ying et al., 2008) and maintaining LIF supplementation (Figure 6I). To confront these two populations, co-cultures were established in the original culture medium only supplemented with LIF. We found that differentiating ESCs are eliminated by co-culture with naive ESCs through CC (Figures 6J and 6K). In addition, the differentiating ESC population displays lower GFP-Myc levels than the naive ESCs population in co-culture (Figures 6L and 6M), confirming correlation between Myc levels and competitive ability. Our results show that Myc levels associate with different states of pluripotency in ESCs and that the co-existence of Myc-high naive ESCs with Myc-low differentiation-primed cells triggers CC for elimination of the latter.

To determine whether spontaneous CC acts as a mechanism to prevent the accumulation of differentiation-primed cells, we blocked cell death by *iMOS*-mediated mosaic expression of the caspase inhibitor p35 (Figure 7A). We analyzed the death-blocked population and found that it shows higher pERK levels than the WT population (Figures 7B and 7C). This result indicates a functional role for cell death in restricting differentiating populations in ESC cultures.

Cell Competition Eliminates Differentiation-Primed Cells from the Epiblast of Pre-gastrulation Mouse Embryos

To determine whether our observations are relevant to epiblast cells in the early mouse embryo, we re-examined the pattern of pERK expression in postimplantation embryos (Corson et al., 2003). The E5 epiblast contained no pERK-positive cells (not shown), whereas the E6 epiblast contained 1%–4% of cells positive for pERK scattered between pERK-negative cells in an apparently random pattern (Figures 7D and 7E). This population of isolated pERK-positive epiblast cells shows lower Myc levels than the pERK-negative population (Figures 7D and 7F), indicating a similar correlation *in vivo* to that found in ESCs. We then studied pERK levels in early gastrulating embryos, where coordinated priming of epiblast cells takes place in the vicinity of the primitive streak for mesoderm formation. We observed regional activation of pERK and downregulation of Myc in epiblast cells close to the primitive streak area (Figure 7G). These observations show that Myc/pERK regulation correlates with epiblast cell differentiation progression, in similarity with the patterns found in ESC cultures. In addition, our observations identify a population of isolated cells that show pERK activation and low Myc levels before differentiation starts in the vicinity of the primitive streak. To determine whether CC functions in the mouse epiblast to restrict this population of early isolated pERK-active cells, we induced p35 mosaic overexpression *in vivo* using the *iMOS* system. We studied E5.5 embryos, in which pERK-activated cells are incipiently detectable in the WT population (Figures 7H and 7I). In these embryos, we observed specific accumulation of pERK-activated cells in the death-blocked p35-overexpressing cells. These results show that cell death eliminates differentiation-primed cells from the pre-gastrulation epiblast.

Myc Directly Determines ESC Competitive Ability without Modifying the Pluripotency Status

To study the functional relationship between Myc levels and the differentiation status, we explored the changes induced upon experimental induction of Myc-high levels in ESCs. We found that *iMOS*-mediated Myc mosaic overexpression, which is enough to induce CC, not only did not lower pERK levels in ESCs but rather induced a mild increase with respect to WT cells, irrespective of whether or not they were in contact with Myc-overexpressing cells (Figures 7J and 7K). We then isolated EYFP-Myc$^+$ and control cells from mosaic cultures and studied their transcriptome in comparison with that of uninduced cells. In Myc-overexpressing cells, we found only small and divergent changes in the expression of two naive pluripotency genes (Figure 7L). Strikingly, we also observed activation of naive pluripotency genes in the WT cell population, which suggests a

Figure 6. The Pluripotency Status Determines Myc Expression Levels and Competitive Ability in ESCs

(A) Top overlaps between gene sets from experiments in ESCs in the MsigDB "chemical and genetic perturbations" database (Subramanian et al., 2005) and the group of genes that change expression between Myc-H and Myc-L cells in RNA-seq analysis.

(B) Principal component analysis between Myc-H, Myc-M, and Myc-L cells, and published expression dataset reports (Buecker et al., 2014; Sasaki et al., 2015) for naive ESCs and epiblast-like stem cells (EPILC).

(C) Analysis of the genes contributing most to PC1; genes functionally involved in pluripotency status regulation or reporting (Guo et al., 2009; Khoa le et al., 2016; Marks et al., 2012; Niwa et al., 2009; Ozmadenci et al., 2015; Ye et al., 2016) are shown in red.

(D) Variations between Myc-H and Myc-L ESCs in the amounts of mRNAs encoding major regulators of pluripotency status. In blue, the core-pluripotency transcription factors; in red, the naive-pluripotency transcription factors; in black, Fgf5, a marker of primed pluripotency.

(E) Co-localization of active pERK and Myc in ESCs.

(F) Active-pERK immunofluorescence signal in ESCs classified by GFP-Myc levels.

(G) Co-localization of pSTAT3 and GFP-Myc in ESCs.

(H) pSTAT3 immunofluorescence signal in ESCs classified by GFP-Myc levels.

(I) Procedure for confronting differentiating ESCs (Tomato$^+$) and naive ESCs (Tomato$^-$). Cultures were established in fetal bovine serum containing the indicated supplements. Co-cultures were prepared at a 1:1 ratio.

(J) Frequency of Tomato$^+$ and Tomato$^-$ cell populations after different periods of co-culture.

(K) Frequency of caspase-3-positive cells in the differentiating Tomato$^+$ cell population alone or in co-culture with naive ESCs. Data were collected by microscopic fields (N).

(L) Immunofluorescence study of Myc levels after 2-day co-culture of Tomato$^-$ ESCs pre-cultured for 3 days with LIF + 2i and Tomato$^+$ ESCs pre-cultured for 3 days without LIF.

(M) GFP-Myc levels in Tomato$^+$ and Tomato$^-$ cell populations in co-culture. Dotplots show means ± 95% confidence interval. Boxplots show median, 25th and 75th percentiles (boxes), 10th and 90th percentiles (whiskers).

Mann-Whitney test was used for boxplots and dotplots. ns, $p > 0.05$, *$p < 0.05$, **$p < 0.01$, ***$p < 0.001$, ****$p < 0.0001$. In (D), ns, adjusted $p > 0.05$; *$p < 0.05$, ***$p < 0.001$. See also Figures S5 and S6.

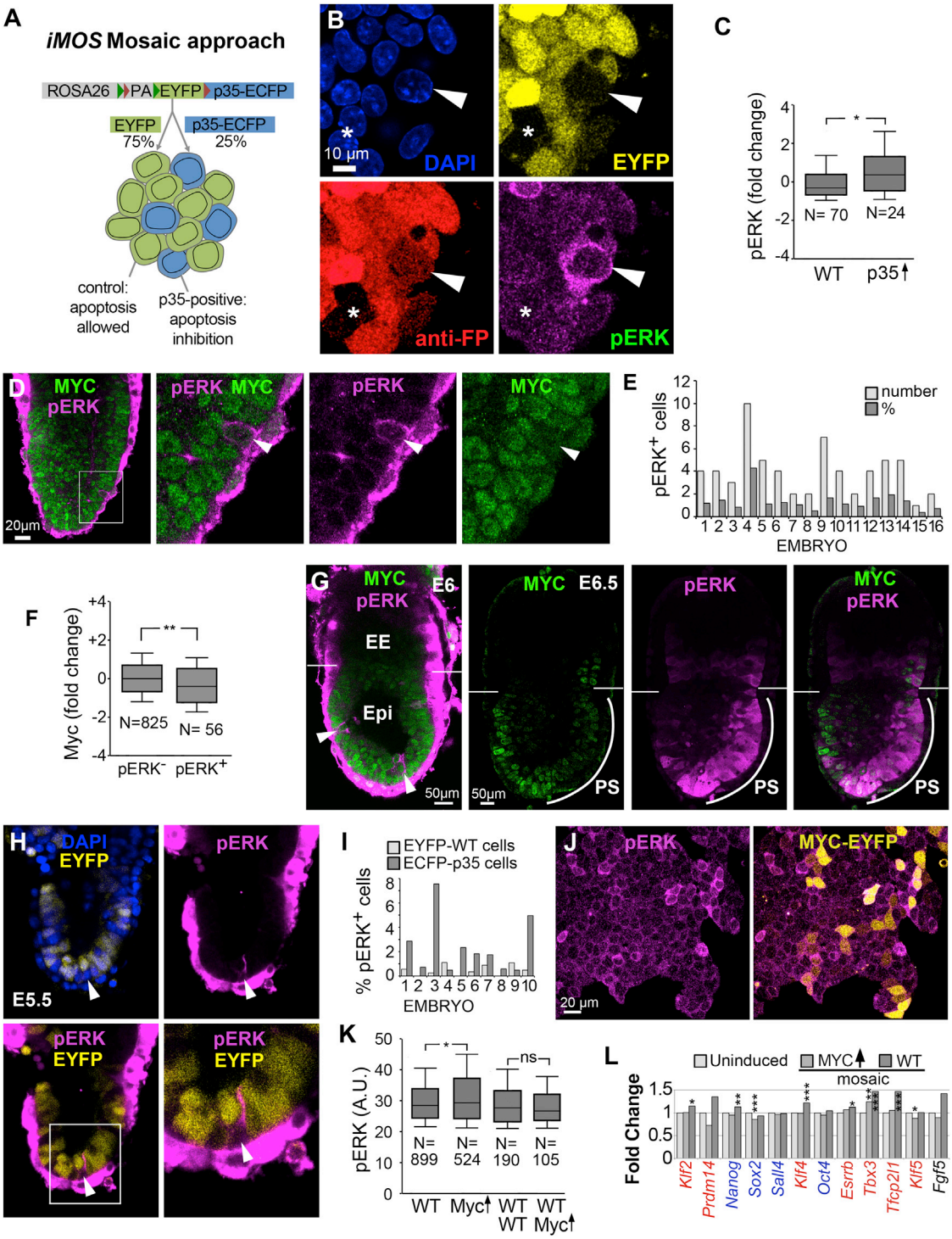

Figure 7. Cell Competition Eliminates Differentiation-Primed Cells from Pluripotent Stem Cell Pools

(A) Scheme showing the *iMOS* strategy for inhibiting CC in ESCs.

(B) Co-localization of direct detection of EYFP with immunofluorescent detection of total fluorescent protein (FP) and active pERK. Arrowheads indicate an ECFP-p35^{+} cell, identified by the absence of EYFP and the presence of FP immunodetection. Asterisks indicate FP-negative cells.

(C) Active-pERK levels fold change in ECFP-p35^{+} cells versus neighboring WT cells.

(D) Co-localization by immunofluorescence of Myc and active pERK in the epiblast of E6 mouse embryos. Arrowheads indicate pERK^{+} cells.

(E) Scoring of active pERK^{+} cells detected in the E6 mouse epiblast.

(F) Normalized Myc-level distributions in active-pERK^{+} and pERK^{-} cells of the mouse E6 epiblast.

(legend continued on next page)

moderate non-autonomous effect of Myc overexpression on the WT cells of the mosaic culture.

Together with the observations that differentiation lowers Myc levels (Figures 6L and 6M) and that *iMOS-Myc* induces the winner phenotype (Clavería et al., 2013), these data indicate a linear pathway in which Myc regulation lies downstream of the differentiation status and Myc levels directly define the competitive ability of ESCs, irrespective of the pluripotency status.

DISCUSSION

Pluripotency is a highly unstable state, yet early mammalian embryos manage to maintain a pool of pluripotent cells for several days. Here, we describe a mechanism that eliminates differentiating ESCs when discrepancies in the differentiation status are present. We also provide evidence for the presence of similar mechanisms acting in the pre-gastrulation mouse epiblast. Competition driven by heterogeneity in differentiation status may be related to the previously reported out competition of BMP receptor-defective cells from ESC populations and the mouse epiblast (Sancho et al., 2013). BMP signaling collaborates with STAT activation in maintaining naive pluripotency, and therefore BMP receptor mutants could be defective in maintaining naive pluripotency, which would lead to Myc downregulation and CC.

Interestingly, only part of the Myc-low ESCs are pERK-high/pSTAT-low; therefore, the differentiation status only explains part of the Myc-low population, and additional cellular features, yet to be identified, should be invoked to completely characterize endogenous CC in the epiblast. Here, the transcriptomic studies identified cell proliferation and metabolic pathways, such as the hypoxia and glycolytic pathways, potentially affecting cell fitness, which will be worth analyzing in the future.

CC induced by discrepancy in differentiation status could operate during phases of early mouse embryo development different from those characterized here. Indeed, cell death has been described starting in the inner cell mass of the blastocyst, much before the stage we have focused on here. Two events of cell differentiation and segregation occur sequentially during preimplantation development: first, trophectoderm cells differentiate and segregate from the undifferentiated cell pool to form the outer layer of the blastocyst; second, the primitive endoderm differentiates and segregates from the inner cell mass of the blastocyst (Stephenson et al., 2012). Interestingly, cells specified as primitive endoderm that fail to segregate from the pluripotent cells of the inner cell mass die by apoptosis (Plusa et al., 2008). Furthermore, Myc is downregulated during primitive endoderm differentiation (Smith et al., 2010), and heterogeneous Myc levels have been reported in the inner cell mass of the blastocyst (Clavería et al., 2013). Although CC has not been explored in the context of primitive endoderm segregation, these observations allow us to speculate that Myc-mediated competition triggered by discrepant differentiation status could be a more general mechanism than that described here. In addition, colonization of the epiblast by ESCs is restricted by apoptosis of differentiation-primed cells (Alexandrova et al., 2016), which would also fit the mechanism described here; however, this elimination was found not to be sensitive to Myc loss of function or related to Myc expression levels (Alexandrova et al., 2016), which would be in contradiction with a direct role of Myc in the inner cell mass or early epiblast CC.

With respect to the dynamics of CC, in ESC cultures Myc-low cells are continuously eliminated and replaced by cells with higher Myc levels. Equilibrium should therefore be maintained by continuous generation of primed cells in ESC cultures, so that new primed cells are compensated by CC-eliminated cells. The fact that Myc-H cells regenerate the Myc-M and Myc-L cells is compatible with this idea, and the observation that this regeneration is a slow process agrees with the high heritability of Myc levels. The fact that Myc-L cells die when replated suggests that this population is stressed in ESC cultures, which is compatible with the model proposed in which loser cells progressively reduce their Myc levels by persistent exposure to Myc-H cells.

Within ESC colonies, interactions between winner and loser cells apparently result from random passive contacts facilitated by the constant movement of ESCs, which results in frequent neighbor exchange and effective cell mixing. During these contacts, we did not detect any obvious active role of either winner or loser cells. This observation contrasts with the involvement of increased cell-mixing activity of winner cells in Myc-induced CC in *Drosophila* imaginal discs (Levayer et al., 2015). *Drosophila* imaginal discs, however, are formed by a columnar epithelium where cells of different lineages mix poorly; therefore, the different environments may explain these differences.

The mechanism characterized here could be important to understand Myc's role during induced pluripotent stem cell generation (Takahashi and Yamanaka, 2006). On one side, our studies add to others showing that Myc activity does not involve cell-autonomous promotion of pluripotency (Gu et al., 2016; Kim et al., 2010; Scognamiglio et al., 2016). Unexpectedly, we found

(G) Co-localization by immunofluorescence of Myc and active pERK in the epiblast of E6 and E6.5 mouse embryos. Arrowheads indicate pERK$^+$ cells. EE, extraembryonic; Epi, epiblast; PS, primitive streak.

(H) Co-localization of EYFP and active-pERK$^+$ cells in the epiblast of E5.5 *iMOS*^{T2p35} mouse embryos recombined with *Sox2Cre*. Arrowheads indicate pERK$^+$ cells.

(I) Scoring of pERK$^+$ cells detected in the epiblast of E5.5 *iMOS*$^{T2\text{-}p35}$ embryos recombined with *Sox2Cre*. p value was calculated by a Wilcoxon matched-pairs signed rank test and refers to the comparison of the distributions of pERK$^+$ cell frequencies in the ECFP$^+$ and ECFP$^-$ cell populations of the embryos scored.

(J) Co-localization of active-pERK and Myc in ESCs with mosaic overexpression of EYFP-Myc from the *iMOS*$^{T1\text{-}Myc}$ allele.

(K) Distributions of active-pERK levels in (from left to right) WT ESCs, ESCs overexpressing EYFP-Myc from the *iMOS*$^{T1\text{-}Myc}$ allele, WT cells in contact only with WT cells, and WT cells in contact with EYFP-Myc-overexpressing cells.

(L) Variations in transcript counts between uninduced *iMOS*^{T1Myc}cells and WT or EYFP-Myc-overexpressing cells after mosaic induction. In blue, the core-pluripotency transcription factors; in red, the naive-pluripotency transcription factors; in black, *Fgf5*, a marker of primed pluripotency.

Boxplots show median, 25th and 75th percentiles (boxes), 10th and 90th percentiles (whiskers). Mann-Whitney test was used for boxplots. ns, $p > 0.05$, *$p < 0.05$, **$p < 0.01$, ***$p < 0.001$. In (L), ns, adjusted $p > 0.05$, *$p < 0.05$, **$p < 0.01$, ***$p < 0.001$.

that Myc mosaic overexpression enhances naive pluripotency marker expression in neighboring WT cells, however this effect was mild and probably has no relevant consequences on reprogramming. In addition, our study suggests that increasing Myc levels during reprogramming may not be very relevant for stimulating proliferation, given that low amounts of Myc protein seem enough to efficiently drive pluripotent cell proliferation. Instead, our findings suggest that during reprogramming, Myc could be involved in promoting the positive selection of pluripotent cells by CC. This view would be compatible with the observation that reprogramming can be achieved without Myc (Nakagawa et al., 2008).

In conclusion, our results reveal a role for endogenous CC in maintaining the naive state in mammalian pluripotent stem cell populations by eliminating cells starting differentiation. The mechanism described here represents a "social" control of the pluripotency status acting at the population level. This mechanism protects pluripotent cell pools by preventing prematurely differentiating cells in a context of predominant naive pluripotent cells. In contrast, coordinated differentiation and Myc downregulation during gastrulation avoid high discrepancies in neighboring cell Myc levels, allowing the exit of cell populations from pluripotency.

STAR★METHODS

Detailed methods are provided in the online version of this paper and include the following:

- KEY RESOURCES TABLE
- CONTACT FOR REAGENT AND RESOURCE SHARING
- EXPERIMENTAL MODEL AND SUBJECT DETAILS
  - mESC Derivation, Modification, and Routine Culture
  - Mouse Lines
- METHOD DETAILS
  - Clonal Analysis Assay
  - *iMOS* Induction for Functional Assays
  - Immunofluorescence
  - Confocal Microscopy
  - Flow Cytometry
  - Time-Lapse Video Microscopy of ESC Cultures
  - RNAseq
  - RNAseq Meta-Analysis
  - 4D Tracking Workflow
- QUANTIFICATION AND STATISTICAL ANALYSIS
- DATA AND SOFTWARE AVAILABILITY

SUPPLEMENTAL INFORMATION

Supplemental Information includes six figures and eight movies and can be found with this article online at http://dx.doi.org/10.1016/j.devcel.2017.08.011.

AUTHOR CONTRIBUTIONS

C.D.D. planned and performed experiments, prepared figures, and wrote the manuscript; L.F.M., D.J.C., and M.C.M. developed the image and data analyses for the 3D + t study; C.C. performed RNA-seq in Myc-overexpression experiments; M.T. planned experiments, prepared figures, and wrote the manuscript.

ACKNOWLEDGMENTS

We thank B. Sleckman for the GFP-Myc mice, the CNIC Microscopy unit for the live confocal analysis, the CNIC Genomics and Bioinformatics units for the RNA-seq analysis, J.C. Alonso for video editing, and M. Manzanares, J.A. Enríquez, and members of the Torres lab for helpful comments on the manuscript. This work was supported by grants BFU2015-71519-P and RD16/0011/0019 (ISCIII) from the Spanish Ministry of Economy, Industry and Competitiveness (MEIC) and grant P2010/BMD-2315 from the Madrid Regional Government to M.T., and grants (BIO2014-62200-EXP) and (PI-FIS-2016) from MEIC to M.C.M. C.D.D. was supported by an FPU grant from the Spanish Ministry of Education, Culture and Sports. The CNIC is supported by the Spanish MEIC and the Pro CNIC Foundation and is a Severo Ochoa Center of Excellence (MEIC award SEV-2015-0505).

Received: April 6, 2017
Revised: June 27, 2017
Accepted: August 15, 2017
Published: September 14, 2017

SUPPORTING CITATIONS

The following reference appears in the Supplemental Information: Liberzon et al. (2015).

REFERENCES

Alexandrova, S., Kalkan, T., Humphreys, P., Riddell, A., Scognamiglio, R., Trumpp, A., and Nichols, J. (2016). Selection and dynamics of embryonic stem cell integration into early mouse embryos. Development *143*, 24–34.

Brons, I.G., Smithers, L.E., Trotter, M.W., Rugg-Gunn, P., Sun, B., Chuva de Sousa Lopes, S.M., Howlett, S.K., Clarkson, A., Ahrlund-Richter, L., Pedersen, R.A., et al. (2007). Derivation of pluripotent epiblast stem cells from mammalian embryos. Nature *448*, 191–195.

Buecker, C., Srinivasan, R., Wu, Z., Calo, E., Acampora, D., Faial, T., Simeone, A., Tan, M., Swigut, T., and Wysocka, J. (2014). Reorganization of enhancer patterns in transition from naive to primed pluripotency. Cell Stem Cell *14*, 838–853.

Cartwright, P., McLean, C., Sheppard, A., Rivett, D., Jones, K., and Dalton, S. (2005). LIF/STAT3 controls ES cell self-renewal and pluripotency by a Myc-dependent mechanism. Development *132*, 885–896.

Chambers, I., Silva, J., Colby, D., Nichols, J., Nijmeijer, B., Robertson, M., Vrana, J., Jones, K., Grotewold, L., and Smith, A. (2007). Nanog safeguards pluripotency and mediates germline development. Nature *450*, 1230–1234.

Clavería, C., Giovinazzo, G., Sierra, R., and Torres, M. (2013). Myc-driven endogenous cell competition in the early mammalian embryo. Nature *500*, 39–44.

Corson, L.B., Yamanaka, Y., Lai, K.M., and Rossant, J. (2003). Spatial and temporal patterns of ERK signaling during mouse embryogenesis. Development *130*, 4527–4537.

Dani, C., Blanchard, J.M., Piechaczyk, M., El Sabouty, S., Marty, L., and Jeanteur, P. (1984). Extreme instability of myc mRNA in normal and transformed human cells. Proc. Natl. Acad. Sci. USA *81*, 7046–7050.

de la Cova, C., Abril, M., Bellosta, P., Gallant, P., and Johnston, L.A. (2004). *Drosophila* myc regulates organ size by inducing cell competition. Cell *117*, 107–116.

Delacroix, L., Moutier, E., Altobelli, G., Legras, S., Poch, O., Choukrallah, M.A., Bertin, I., Jost, B., and Davidson, I. (2010). Cell-specific interaction of retinoic acid receptors with target genes in mouse embryonic fibroblasts and embryonic stem cells. Mol. Cell. Biol. *30*, 231–244.

Evans, M.J., and Kaufman, M.H. (1981). Establishment in culture of pluripotential cells from mouse embryos. Nature *292*, 154–156.

Fernández-de-Manuel, L., Diaz-Diaz, C., Jimenez-Carretero, D., Torres, M., and Montoya, M.C. (2017). ESC-Track: a computer workflow for 4-D segmentation, tracking, lineage tracing and dynamic context analysis of ESCs. Biotechniques *62*, 215–222.

Gopinath, S., Wen, Q., Thakoor, N., Luby-Phelps, K., and Gao, J.X. (2008). A statistical approach for intensity loss compensation of confocal microscopy images. J. Microsc. *230*, 143–159.

Gu, W., Gaeta, X., Sahakyan, A., Chan, A.B., Hong, C.S., Kim, R., Braas, D., Plath, K., Lowry, W.E., and Christofk, H.R. (2016). Glycolytic metabolism plays a functional role in regulating human pluripotent stem cell state. Cell Stem Cell *19*, 476–490.

Guerra, C., Mijimolle, N., Dhawahir, A., Dubus, P., Barradas, M., Serrano, M., Campuzano, V., and Barbacid, M. (2003). Tumor induction by an endogenous K-ras oncogene is highly dependent on cellular context. Cancer Cell *4*, 111–120.

Guo, G., Yang, J., Nichols, J., Hall, J.S., Eyres, I., Mansfield, W., and Smith, A. (2009). Klf4 reverts developmentally programmed restriction of ground state pluripotency. Development *136*, 1063–1069.

Hann, S.R., and Eisenman, R.N. (1984). Proteins encoded by the human c-myc oncogene: differential expression in neoplastic cells. Mol. Cell. Biol. *4*, 2486–2497.

Hayashi, S., Lewis, P., Pevny, L., and McMahon, A.P. (2002). Efficient gene modulation in mouse epiblast using a Sox2Cre transgenic mouse strain. Mech. Dev. *119* (*Suppl 1*), S97–S101.

Hayashi, K., Ohta, H., Kurimoto, K., Aramaki, S., and Saitou, M. (2011). Reconstitution of the mouse germ cell specification pathway in culture by pluripotent stem cells. Cell *146*, 519–532.

Heyer, B.S., MacAuley, A., Behrendtsen, O., and Werb, Z. (2000). Hypersensitivity to DNA damage leads to increased apoptosis during early mouse development. Genes Dev. *14*, 2072–2084.

Hu, G., Kim, J., Xu, Q., Leng, Y., Orkin, S.H., and Elledge, S.J. (2009). A genome-wide RNAi screen identifies a new transcriptional module required for self-renewal. Genes Dev. *23*, 837–848.

Huang, C.Y., Bredemeyer, A.L., Walker, L.M., Bassing, C.H., and Sleckman, B.P. (2008). Dynamic regulation of c-Myc proto-oncogene expression during lymphocyte development revealed by a GFP-c-Myc knock-in mouse. Eur. J. Immunol. *38*, 342–349.

Kalmar, T., Lim, C., Hayward, P., Munoz-Descalzo, S., Nichols, J., Garcia-Ojalvo, J., and Martinez Arias, A. (2009). Regulated fluctuations in nanog expression mediate cell fate decisions in embryonic stem cells. PLoS Biol. *7*, e1000149.

Khoa le, T.P., Azami, T., Tsukiyama, T., Matsushita, J., Tsukiyama-Fujii, S., Takahashi, S., and Ema, M. (2016). Visualization of the epiblast and visceral endodermal cells using Fgf5-P2A-venus BAC transgenic mice and epiblast stem cells. PLoS One *11*, e0159246.

Kim, J., Woo, A.J., Chu, J., Snow, J.W., Fujiwara, Y., Kim, C.G., Cantor, A.B., and Orkin, S.H. (2010). A Myc network accounts for similarities between embryonic stem and cancer cell transcription programs. Cell *143*, 313–324.

Kunath, T., Saba-El-Leil, M.K., Almousailleakh, M., Wray, J., Meloche, S., and Smith, A. (2007). FGF stimulation of the Erk1/2 signalling cascade triggers transition of pluripotent embryonic stem cells from self-renewal to lineage commitment. Development *134*, 2895–2902.

Levayer, R., Hauert, B., and Moreno, E. (2015). Cell mixing induced by myc is required for competitive tissue invasion and destruction. Nature *524*, 476–480.

Li, B., and Dewey, C.N. (2011). RSEM: accurate transcript quantification from RNA-Seq data with or without a reference genome. BMC Bioinformatics *12*, 323.

Liberzon, A., Birger, C., Thorvaldsdottir, H., Ghandi, M., Mesirov, J.P., and Tamayo, P. (2015). The Molecular Signatures Database (MSigDB) hallmark gene set collection. Cell Syst. *1*, 417–425.

Marks, H., Kalkan, T., Menafra, R., Denissov, S., Jones, K., Hofemeister, H., Nichols, J., Kranz, A., Stewart, A.F., Smith, A., et al. (2012). The transcriptional and epigenomic foundations of ground state pluripotency. Cell *149*, 590–604.

Martello, G., and Smith, A. (2014). The nature of embryonic stem cells. Annu. Rev. Cell Dev. Biol. *30*, 647–675.

Martin, G.R. (1981). Isolation of a pluripotent cell line from early mouse embryos cultured in medium conditioned by teratocarcinoma stem cells. Proc. Natl. Acad. Sci. USA *78*, 7634–7638.

Martin, M. (2011). Cutadapt removes adapter sequences from high-throughput sequencing reads. EMBnet.journal *17*, 10–12.

Morata, G., and Ripoll, P. (1975). Minutes: mutants of drosophila autonomously affecting cell division rate. Dev. Biol. *42*, 211–221.

Moreno, E., and Basler, K. (2004). dMyc transforms cells into super-competitors. Cell *117*, 117–129.

Nakagawa, M., Koyanagi, M., Tanabe, K., Takahashi, K., Ichisaka, T., Aoi, T., Okita, K., Mochiduki, Y., Takizawa, N., and Yamanaka, S. (2008). Generation of induced pluripotent stem cells without Myc from mouse and human fibroblasts. Nat. Biotechnol. *26*, 101–106.

Nichols, J., and Smith, A. (2009). Naive and primed pluripotent states. Cell Stem Cell *4*, 487–492.

Niwa, H., Burdon, T., Chambers, I., and Smith, A. (1998). Self-renewal of pluripotent embryonic stem cells is mediated via activation of STAT3. Genes Dev. *12*, 2048–2060.

Niwa, H., Ogawa, K., Shimosato, D., and Adachi, K. (2009). A parallel circuit of LIF signalling pathways maintains pluripotency of mouse ES cells. Nature *460*, 118–122.

Ozmadenci, D., Feraud, O., Markossian, S., Kress, E., Ducarouge, B., Gibert, B., Ge, J., Durand, I., Gadot, N., Plateroti, M., et al. (2015). Netrin-1 regulates somatic cell reprogramming and pluripotency maintenance. Nat. Commun. *6*, 7398.

Plusa, B., Piliszek, A., Frankenberg, S., Artus, J., and Hadjantonakis, A.K. (2008). Distinct sequential cell behaviours direct primitive endoderm formation in the mouse blastocyst. Development *135*, 3081–3091.

Poelmann, R.E. (1980). Differential mitosis and degeneration patterns in relation to the alterations in the shape of the embryonic ectoderm of early post-implantation mouse embryos. J. Embryol. Exp. Morphol. *55*, 33–51.

Robinson, M.D., McCarthy, D.J., and Smyth, G.K. (2010). edgeR: a Bioconductor package for differential expression analysis of digital gene expression data. Bioinformatics *26*, 139–140.

Rossant, J. (2008). Stem cells and early lineage development. Cell *132*, 527–531.

Sancho, M., Di-Gregorio, A., George, N., Pozzi, S., Sanchez, J.M., Pernaute, B., and Rodriguez, T.A. (2013). Competitive interactions eliminate unfit embryonic stem cells at the onset of differentiation. Dev. Cell *26*, 19–30.

Sasaki, K., Yokobayashi, S., Nakamura, T., Okamoto, I., Yabuta, Y., Kurimoto, K., Ohta, H., Moritoki, Y., Iwatani, C., Tsuchiya, H., et al. (2015). Robust in vitro induction of human germ cell fate from pluripotent stem cells. Cell Stem Cell *17*, 178–194.

Scognamiglio, R., Cabezas-Wallscheid, N., Thier, M.C., Altamura, S., Reyes, A., Prendergast, A.M., Baumgartner, D., Carnevalli, L.S., Atzberger, A., Haas, S., et al. (2016). Myc depletion induces a pluripotent dormant state mimicking diapause. Cell *164*, 668–680.

Smith, A.G., Heath, J.K., Donaldson, D.D., Wong, G.G., Moreau, J., Stahl, M., and Rogers, D. (1988). Inhibition of pluripotential embryonic stem cell differentiation by purified polypeptides. Nature *336*, 688–690.

Smith, K.N., Singh, A.M., and Dalton, S. (2010). Myc represses primitive endoderm differentiation in pluripotent stem cells. Cell Stem Cell *7*, 343–354.

Stephenson, R.O., Rossant, J., and Tam, P.P. (2012). Intercellular interactions, position, and polarity in establishing blastocyst cell lineages and embryonic axes. Cold Spring Harb. Perspect. Biol. *4*, http://dx.doi.org/10.1101/cshperspect.a008235.

Subramanian, A., Tamayo, P., Mootha, V.K., Mukherjee, S., Ebert, B.L., Gillette, M.A., Paulovich, A., Pomeroy, S.L., Golub, T.R., Lander, E.S., et al. (2005). Gene set enrichment analysis: a knowledge-based approach for interpreting genome-wide expression profiles. Proc. Natl. Acad. Sci. USA *102*, 15545–15550.

Takahashi, K., and Yamanaka, S. (2006). Induction of pluripotent stem cells from mouse embryonic and adult fibroblast cultures by defined factors. Cell *126*, 663–676.

Tesar, P.J., Chenoweth, J.G., Brook, F.A., Davies, T.J., Evans, E.P., Mack, D.L., Gardner, R.L., and McKay, R.D. (2007). New cell lines from mouse epiblast share defining features with human embryonic stem cells. Nature *448*, 196–199.

van Oosten, A.L., Costa, Y., Smith, A., and Silva, J.C. (2012). JAK/STAT3 signalling is sufficient and dominant over antagonistic cues for the establishment of naive pluripotency. Nat. Commun. *3*, 817.

Villa del Campo, C., Claveria, C., Sierra, R., and Torres, M. (2014). Cell competition promotes phenotypically silent cardiomyocyte replacement in the mammalian heart. Cell Rep. *8*, 1741–1751.

Wang, J., Rao, S., Chu, J., Shen, X., Levasseur, D.N., Theunissen, T.W., and Orkin, S.H. (2006). A protein interaction network for pluripotency of embryonic stem cells. Nature *444*, 364–368.

Welcker, M., Orian, A., Jin, J., Grim, J.E., Harper, J.W., Eisenman, R.N., and Clurman, B.E. (2004). The Fbw7 tumor suppressor regulates glycogen synthase kinase 3 phosphorylation-dependent c-Myc protein degradation. Proc. Natl. Acad. Sci. USA *101*, 9085–9090.

Yamazaki, K., Aso, T., Ohnishi, Y., Ohno, M., Tamura, K., Shuin, T., Kitajima, S., and Nakabeppu, Y. (2003). Mammalian elongin A is not essential for cell viability but is required for proper cell cycle progression with limited alteration of gene expression. J. Biol. Chem. *278*, 13585–13589.

Ye, S., Zhang, D., Cheng, F., Wilson, D., Mackay, J., He, K., Ban, Q., Lv, F., Huang, S., Liu, D., et al. (2016). Wnt/beta-catenin and LIF-Stat3 signaling pathways converge on Sp5 to promote mouse embryonic stem cell self-renewal. J. Cell Sci. *129*, 269–276.

Ying, Q.L., Nichols, J., Chambers, I., and Smith, A. (2003). BMP induction of Id proteins suppresses differentiation and sustains embryonic stem cell self-renewal in collaboration with STAT3. Cell *115*, 281–292.

Ying, Q.L., Wray, J., Nichols, J., Batlle-Morera, L., Doble, B., Woodgett, J., Cohen, P., and Smith, A. (2008). The ground state of embryonic stem cell self-renewal. Nature *453*, 519–523.

STAR★METHODS

KEY RESOURCES TABLE

REAGENT or RESOURCE	SOURCE	IDENTIFIER
Antibodies		
anti-Myc polyclonal antibody	Millipore	06-340
anti-Myc T58	abcam	ab85380
phospho-p44/42 MAPK (Erk1/2) (Thr202/Tyr204)	Cell Signaling	#4370
anti-phospho-histone H3 (Ser 10) 'mitosis marker'	Millipore	06-570
Phospho-Histone H3 (Ser10) (6G3)	Cell Signaling	#9706
cleaved-caspase3 (Asp175) Antibody	Cell Signaling	#9661
phospho-Stat3 (Tyr705) D3A7, Cell Signaling	Cell Signaling	#9145
anti-GFP	Aves Lab	GFP-1010
phospho-p44/42 MAPK (Erk1/2) (Thr202/Tyr204)	Cell Signaling	#9106
Phospho-Histone H2AX (Ser139)	Millipore	05-636
p53 (1C12)	Cell Signaling	#2524S
Chemicals, Peptides, and Recombinant Proteins		
4-hydroxytamoxifen	Sigma-Aldrich	H7904
Stemolecule CHIR99021	Stemgent	04-0004-02
Stemolecule PD0325901	Stemgent	04-0006
Hoechst33258	Sigma-Aldrich	B2883
Propidium iodide	Sigma-Aldrich	P4864
Critical Commercial Assays		
CaspGLOW^{TM} Red Caspase Staining kit	MBL international	JM-K190-25
QIAGEN RNa-easy Mini Kit	Qiagen	74104
Deposited Data		
Complete sets of raw data used in this publication	Mendeley	https://data.mendeley.com/datasets/fjxw65r3m2/draft?a=0e0569ad-389e-409f-ae27-7e3fbe50b851
RNA-seq datasets from this publication	Gene Expression Omnibus	GSE89196 and GSE100570
RNA-seq dataset from Sasaki et al., 2015	Gene Expression Omnibus	GSE67259
RNA-seq dataset from Buecker et al., 2014	Gene Expression Omnibus	GSE56138
Experimental Models: Cell Lines		
iMOS$^{T2\text{-}p35}$ mouse ESCs	This paper	N/A
iMOS^{WT} mouse ESCs	This paper	N/A
iMOS$^{T1\text{-}Myc}$ mouse ESCs	This paper	N/A
GFP-Myc mouse ESCs	This paper	N/A
		N/A
Experimental Models: Organisms/Strains		
GFP-Myc mouse strain	Huang et al., 2008	N/A
CD1 mouse strain	Originally from Charles River and then bred at CNIC facilities for about one year	Crl:CD1(ICR)
iMOS$^{T2\text{-}p35}$ mouse strain	Clavería et al., 2013	N/A
Sox2Cre mouse strain	Hayashi et al., 2002	N/A
Software and Algorithms		
ESC-Track	Fernández-de-Manuel et al., 2017	Available at: https://www.cnic.es/en/investigacion/2/1186/tecnologia
FIJI (ImageJ)	NIH	Image J version 2

(*Continued on next page*)

Continued

REAGENT or RESOURCE	SOURCE	IDENTIFIER
Prism	GraphPad	version 5.0
NCSS 11 Statistical Software	NCSS, LLC.	2016
Imaris	Bitplane	version 7.2.3
BD FACSDiva Software	BD Biosciences	version 6.1.2
Excel	Microsoft	2016
Definiens Developer	Definiens	version XD2.4
Matlab	The MathWorks, Inc.	R2015a
FastQC	Babraham Informatics	N/A
RSEM (Li and Dewey, 2011)	Li and Dewey	v1.2.3 (Li and Dewey, 2011)
Bioconductor package EdgeR	Robinson et al., 2010	N/A
Cutadapt	Martin, 2011	v1.3
Other		
GAII Analyzer	Illumina	N/A

CONTACT FOR REAGENT AND RESOURCE SHARING

Further information and requests for resources and reagents should be directed to and will be fulfilled by the Lead Contact Miguel Torres (mtorres@cnic.es).

EXPERIMENTAL MODEL AND SUBJECT DETAILS

mESC Derivation, Modification, and Routine Culture

mESCs were derived from E3.5 blastocysts following the 2i derivation protocol (GSK3β and Mek 1/2 inhibitors). Cultures were checked for Mycoplasma and normal karyotype at their establishment. The heterozygous *iMOS*^{WT} and *iMOS*$^{T1\text{-}Myc}$ and homozygous *iMOS*$^{T2\text{-}p35}$ ESC lines were derived from previously described *iMOS* mice (Clavería et al., 2013). For time-lapse studies, the ESC lines were stably transfected with a PGK-tdTomato construct that drives expression of a membrane-attached Tomato fluorescent protein. ESCs were routinely maintained on mitoMycin-C-inactivated mouse embryonic fibroblast (MEF) feeder layers. ESC routine culture medium (SR-ES medium) contained high glucose DMEM, GlutaMAX™, KO-Serum Replacement (Invitrogen), Pyruvate (LifeTech), LIF, 1x nonessential amino acids and 2-beta-mercaptoethanol.

Mouse Lines

The GFP-Myc mouse line has been described previously (Huang et al., 2008). Homozygous mice are viable and show no apparent phenotypic alterations. Wild type mice used were of the CD1 strain. The *iMOS*$^{T2\text{-}p35}$ mouse line has been previously described (Clavería et al., 2013). For activation, *iMOS*$^{T2\text{-}p35}$ mice were crossed to *Sox2Cre* mice (Hayashi et al., 2002).

METHOD DETAILS

Clonal Analysis Assay

150,000 ESCs were plated without feeder on fibronectin-coated 3.5-mm glass bottom dishes (MatTek) and cultured in 2xLIF SR-ES medium. To generate clones we used the *RERT*; *iMOS*^{WT} cell line (Clavería et al., 2013) and induced EYFP clones at a very low recombination rate. For this cells were treated 48h after plating for 1 h with 5 μM 4-hydroxytamoxifen (4-OHTAM) (Sigma-Aldrich) and cultured for an additional 60h. Only 15% of colonies were recombined, so the expected frequency of polyclonal groups was around 2% (0.15^2X100). Cells were fixed and analyzed by confocal immunofluorescence for Myc, and subject to confocal analysis. We then calculated the variation of Myc levels within clonal groups identified by EYFP signal and for a set of equivalent randomly chosen cell groups. We repeated the process of random group generation at least 100 times per colony to have a sample representative of the whole population and considered the median standard deviation of the 100 subsamples.

iMOS Induction for Functional Assays

For *iMOS*$^{T1\text{-}Myc}$ and *iMOS*$^{T2\text{-}p35}$ induction, cells were plated without feeder on fibronectin-coated 3.5-mm glass bottom dishes (MatTek) and cultured in 2xLIF SR-ES medium. After 24h *iMOS*$^{T1\text{-}Myc}$ cells were treated with 10 μM 4-hydroxytamoxifen (4-OHTAM) (Sigma-Aldrich) and *iMOS*$^{T2\text{-}p35}$ cells with 20 μM for 24 h and cultured for additional 24 h.

Immunofluorescence

For all mESC immunostaining assays, cells were plated at low density without feeder on fibronectin-coated 3.5-mm glass bottom dishes (MatTek) and cultured in 2xLIF SR-ES medium. Cells were fixed overnight in 2% paraformaldehyde (PFA) in PBS at 4°C, blocked in PBS containing 10% goat serum and 0.1% Triton-X 100, and incubated with the following antibodies in blocking solution for 1 h at room temperature or over-night at 4°C: anti-Myc polyclonal antibody, dilution 1:300 (06-340, Millipore); anti-Myc T58, dilution 1:100 (ab85380, abcam), phospho-p44/42 MAPK (Erk1/2) (Thr202/Tyr204), dilution 1:200 (#4370, Cell Signaling), anti-phospho-histone H3 (Ser 10) 'mitosis marker', dilution 1:300 (06-570, Millipore), Phospho-Histone H3 (Ser10) (6G3), dilution 1:300 (#9706, Cell Signaling), cleaved-caspase3 (Asp175) Antibody, dilution 1:100 (#9661 Cell Signaling), phospho-Stat3 (Tyr705) D3A7, dilution 1:100 (#9145, Cell Signaling), anti-GFP, dilution 1:500 (GFP-1010; Aves Lab), p53 (1C12), dilution 1:500 (#2524S, Cell Signaling), Phospho-Histone H2AX (Ser139), dilution 1:200 (05-636, Millipore). Mouse embryos were fixed overnight in 2% PFA in PBS at 4°C and incubated with anti-Myc polyclonal antibody, dilution 1:300 (06-340, Millipore) and phospho-p44/42 MAPK (Erk1/2) (Thr202/Tyr204), dilution 1:200 (#9106 or #4370, Cell Signaling) in blocking solution over-night at 4°C.

Confocal Microscopy

Immunofluorescence of fixed cells was imaged with either a Leica TCS SP5 inverted conventional confocal microscope fitted with a HCX PL APO CS 40x 1.25 oil objective, an SP8 inverted conventional confocal microscope fitted with HC PL Apo CS2 40x/1.3 oil objective, or a Zeiss LSM 780 upright microscope fitted with W Plan-Apochromat 40x/1,0 DIC M27 objective. Whole mouse embryos were imaged with a Zeiss LSM 780 upright microscope fitted with a W Plan-Apochromat 20x/1,0 DIC M27 75mm WD 1.8mm objective in confocal mode at 405, 488, 568 or 663 nm.

Flow Cytometry

For the LIF withdrawal assay, cells were trypsinized, resuspended in 2%FBS PBS and stained with Hoechst33258 (B-2883, Sigma) for dead cell exclusion. Cell suspensions were analysed in a BD LSRFortessa Special Order Research Product. For cell cycle analysis, cells were trypsinized, incubated in culture medium with 5 μg/ml Hoechst33342 (B2261-Sigma) for 45 minutes at 37°C, washed and resuspended in 2%FBS PBS and analysed by flow cytometry in a BD FACSCanto II. Propidium iodide (P4864-Sigma) was used to identify dead cells.

Time-Lapse Video Microscopy of ESC Cultures

200,000 ESCs were seeded on 3.5-mm 0.1% gelatine-coated plastic plates (Falcon) without feeder and cultured in 2xLIF SR-ES medium. 24 h later cells were transferred to the environmental chamber of a Zeiss LSM 780 upright microscope. In every imaging experiment, the incubation chamber was previously stabilised to 37°C and 5% CO2 by mixing and humidification. To avoid liquid evaporation, embryo-grade mineral oil was added on top of the medium after objective immersion. Samples were imaged with a W Plan-Apochromat 40x/1,0 DIC M27 objective every 7 minutes for 24 h. Z-stacks with sections spaced at 2 μm were acquired at each timepoint. In addition, a multi-position map was generated, and every ESC colony was manually assigned an x-y-z location. We used confocal lasers with two excitation channels (488 nm excitation for GFP-Myc visualization and 561 nm excitation for the tdTomato membrane marker), and all images were 512x512 pixels (0.415x0.415 μm resolution), taken at speed 7 and with 2 scans/Z-slice. A trade-off between spatial resolution, temporal resolution and total acquisition time was carefully selected to minimize photobleaching while enabling tracking of cell division, apoptosis and cell-cell interactions. For apoptosis detection we added either Hoechst33258 (B-2883, Sigma) (1:2000) or caspase3-reporter (CaspGLOW Red Caspase Staining kit, MBL) (1:1000) to the medium immediately before imaging.

For $iMOS^{T1\text{-}Myc}$ induction analyses, we started time-lapse confocal analysis 10 h after the induction. The timings of new $EYFP^{+}$ cells and apoptotic events were scored manually. The complete set of raw videos used in this work are available as specified in the "Data and software availability" section.

RNAseq

For RNA-seq, total RNA was purified from ES cells sorted in a cytometer according to GFP-Myc or EYFP levels (three biological replicas). RNA from ES cell population was extracted and purified using Qiagen RNeasy Mini Kit extraction (QIAGEN). A cDNA library was prepared according to Illumina recommendations and sequenced in a GAII analyzer using the paired-end 50bp protocol. Sequencing reads were pre-processed by means of a pipeline that used FastQC to asses read quality, and Cutadapt v1.3 (Martin, 2011) to trim sequencing reads, eliminating Illumina adaptor remains and discarding reads shorter than 30 bp. Reads were mapped against the mouse transcriptome (GRCm38 assembly, Ensembl release 76) and quantified using RSEM v1.2.3 (Li and Dewey, 2011). Raw data have been deposited in the GEO database with reference numbers GSE89196 and GSE100570. Raw expression counts were then processed with an analysis pipeline that used the Bioconductor package EdgeR (Robinson et al., 2010) for normalization and differential expression testing. Only genes expressed at a minimal level of 1 count per million, in at least 3 samples, were considered for differential expression analysis.

RNAseq Meta-Analysis

Gene set enrichment analysis was performed using the online tools in the Broad Institute GSEA web site (http://software.broadinstitute.org/gsea/). Genes with significant variation between Myc-H and Myc-L cells (adj pval <0.001) were screened against

the curated ''chemical and genetic perturbations'' from MsigDB. In addition, genes upregulated in Myc-L cells (adj pval <0.001) were screened against the ''hallmark'' gene sets from MsigDB.

For Principal Components Analysis, we compared our RNA-seq dataset to Gene Expression Omnibus RNA-Seq datasets GSE67259 and GSE56138. For GSE67259 dataset, expression levels in RPMs were compared with the TPMs calculated from FPKMs of dataset GSE56138 and to the TPMs of our dataset. For each gene symbol we considered the TPMs of all samples from all datasets. 16,998 genes were expressed in all experiments. Combat (Robinson et al., 2010) without covariate was then used on the log2-TPMs matrix to remove batch differences among the datasets. ggfortify and gplots packages were used for visualization of the Principal Components Analysis and main gene set contributing to the Principal Component 1.

4D Tracking Workflow

Image processing and analysis methods were developed using Definiens Developer version XD2.4 (Definiens AG, Germany) and Matlab (R2015a, Bioinformatics, Image Processing, Optimization, Statistics and Machine Learning toolboxes). A manual editing tool was implemented, allowing the user to visualize and correct errors. Quantitative cellular parameters in the pipeline are automatically extracted from the segmented and tracked nuclei, generating tables ready for data mining. The tables contain information on cell and nuclear position and shape, nuclear GFP intensity, cell neighborhood, nuclear size, mitosis and apoptosis. The complete set of primary measurements generated is available in table format, as specified in the ''Data and software availability'' section.

During time-lapse analysis, photobleaching of GFP-Myc fluorescence produced a progressive signal reduction throughout the first third of the tracking period (Figure S4). After the initial photobleaching, the GFP-Myc signal was stable during the remainder of the tracking period (Figure S4). To avoid interference from photobleaching during the analysis, we adapted established methods (Gopinath et al., 2008) to normalize the values, using the endpoint mean and standard deviation as reference values (Fernández-de-Manuel et al., 2017). All quantitative analyses were made using the normalized data. This procedure allowed to perform meaningful *in silico* synchronizations. The procedures used for 4D tracking and quantitative analysis have been published in full detail in (Fernández-de-Manuel et al., 2017).

QUANTIFICATION AND STATISTICAL ANALYSIS

Statistical analyses were performed using Prism v5.0 and have been included in Figure legends.

DATA AND SOFTWARE AVAILABILITY

The complete sets of raw data used in this publication are available from Mendeley (https://data.mendeley.com/datasets/fjxw65r3m2/draft?a=0e0569ad-389e-409f-ae27-7e3fbe50b851), except RNAseq data, which have been deposited in the GEO database with reference numbers GEO: GSE89196 and GSE100570.